

Quantum Monte-Carlo Studies of Generalized Many-body Systems

Jørgen Høgberget

June 17, 2013

Goals

- Develop a *general* Quantum Monte-Carlo (QMC) solver for *many-body* systems.

Goals

- Develop a *general* Quantum Monte-Carlo (QMC) solver for *many-body* systems.
 - Achieved through ~ 15000 lines of object oriented C++.

Goals

- Develop a *general* Quantum Monte-Carlo (QMC) solver for *many-body* systems.
 - Achieved through ~ 15000 lines of object oriented C++.
 - 5000 of which were auto-generated by *SymPy*.

Goals

- Develop a *general* Quantum Monte-Carlo (QMC) solver for *many-body* systems.
 - Achieved through ~ 15000 lines of object oriented C++.
 - 5000 of which were auto-generated by *SymPy*.
 - Large focus on optimizations.

Goals

- Develop a *general* Quantum Monte-Carlo (QMC) solver for *many-body* systems.
 - Achieved through ~ 15000 lines of object oriented C++.
 - 5000 of which were auto-generated by *SymPy*.
 - Large focus on optimizations.
 - Additional focus on software solutions for handling extreme amounts of data.

Goals

- Develop a *general* Quantum Monte-Carlo (QMC) solver for *many-body* systems.
 - Achieved through ~ 15000 lines of object oriented C++.
 - 5000 of which were auto-generated by *SymPy*.
 - Large focus on optimizations.
 - Additional focus on software solutions for handling extreme amounts of data.
 - Focus on readability and being easy to extend.

Goals

- Develop a *general* Quantum Monte-Carlo (QMC) solver for *many-body* systems.
 - Achieved through ~ 15000 lines of object oriented C++.
 - 5000 of which were auto-generated by *SymPy*.
 - Large focus on optimizations.
 - Additional focus on software solutions for handling extreme amounts of data.
 - Focus on readability and being easy to extend.
- Implement several well-known systems and provide *preliminary* results.

Goals

- Develop a *general* Quantum Monte-Carlo (QMC) solver for *many-body* systems.
 - Achieved through ~ 15000 lines of object oriented C++.
 - 5000 of which were auto-generated by *SymPy*.
 - Large focus on optimizations.
 - Additional focus on software solutions for handling extreme amounts of data.
 - Focus on readability and being easy to extend.
- Implement several well-known systems and provide *preliminary* results.
 - Total of five systems simulated for up to 56 particles and 108 degrees of freedom.

Goals

- Develop a *general* Quantum Monte-Carlo (QMC) solver for *many-body* systems.
 - Achieved through ~ 15000 lines of object oriented C++.
 - 5000 of which were auto-generated by *SymPy*.
 - Large focus on optimizations.
 - Additional focus on software solutions for handling extreme amounts of data.
 - Focus on readability and being easy to extend.
- Implement several well-known systems and provide *preliminary* results.
 - Total of five systems simulated for up to 56 particles and 108 degrees of freedom.
 - Efficient simulations on both large scales (abel) and smaller scales (single computational nodes)

Contents

- 1 The basics of Quantum Monte-Carlo
- 2 Results and Discussions

The basic idea

- Project an arbitrary state down on the exact ground state.
- Model this state by an ensemble of random walkers.
- Simulate the projection using stochastic processes.

The projection

$$\hat{\mathbf{P}}(\tau) = \exp(-(\hat{\mathbf{H}} - E_0)\tau)$$

$$\hat{\mathbf{P}}(\tau) |\Psi_T\rangle = C_0 |\Psi_0\rangle + \sum_{k=1} \mathcal{C}_k \exp(-\Delta E_k \tau) |\Psi_k\rangle$$

where $\Delta E_k > 0$ and $C_k = \langle \Psi_k | \Psi_T \rangle$.

The projection

$$\hat{\mathbf{P}}(\tau) = \exp(-(\hat{\mathbf{H}} - E_0)\tau)$$

$$\hat{\mathbf{P}}(\tau) |\Psi_T\rangle = C_0 |\Psi_0\rangle + \sum_{k=1} C_k \exp(-\Delta E_k \tau) |\Psi_k\rangle$$

where $\Delta E_k > 0$ and $C_k = \langle \Psi_k | \Psi_T \rangle$.

In other words

$$\lim_{\tau \rightarrow \infty} \langle \mathbf{r} | \hat{\mathbf{P}}(\tau) | \Psi_T \rangle = \langle \Psi_0 | \Psi_T \rangle \Psi_0(\mathbf{r}).$$

The stochastic process

In order to relate the projection process to a *Markov chain* Monte-Carlo process, τ needs to be split into sequential steps $\delta\tau$.

The stochastic process

In order to relate the projection process to a *Markov chain* Monte-Carlo process, τ needs to be split into sequential steps $\delta\tau$.

Using that

$$\hat{\mathbf{P}}(\tau + \delta\tau) = \exp(-(\hat{\mathbf{H}} - E_0)\delta\tau)\hat{\mathbf{P}}(\tau),$$

yields

$$\begin{aligned}\Phi(\mathbf{r}, \tau + \delta\tau) &\equiv \langle \mathbf{r} | \hat{\mathbf{P}}(\tau + \delta\tau) | \Psi_T \rangle \\ &= \int_{\mathbf{r}'} \langle \mathbf{r} | \exp(-(\hat{\mathbf{H}} - E_0)\delta\tau) | \mathbf{r}' \rangle \Phi(\mathbf{r}', \tau) d\mathbf{r}',\end{aligned}$$

The stochastic process

In order to relate the projection process to a *Markov chain* Monte-Carlo process, τ needs to be split into sequential steps $\delta\tau$.

Using that

$$\hat{\mathbf{P}}(\tau + \delta\tau) = \exp(-(\hat{\mathbf{H}} - E_0)\delta\tau)\hat{\mathbf{P}}(\tau),$$

yields

$$\begin{aligned}\Phi(\mathbf{r}, \tau + \delta\tau) &\equiv \langle \mathbf{r} | \hat{\mathbf{P}}(\tau + \delta\tau) | \Psi_T \rangle \\ &= \int_{\mathbf{r}'} \langle \mathbf{r} | \exp(-(\hat{\mathbf{H}} - E_0)\delta\tau) | \mathbf{r}' \rangle \Phi(\mathbf{r}', \tau) d\mathbf{r}',\end{aligned}$$

$$\langle \mathbf{r} | \exp(-(\hat{\mathbf{H}} - E_0)\delta\tau) | \mathbf{r}' \rangle \equiv G(\mathbf{r}', \mathbf{r}; \delta\tau).$$

The stochastic process

In order to relate the Green's function to well known Markov processes, the exponential is split

$$\begin{aligned}\exp(-(\hat{\mathbf{H}} - E_0)\delta\tau) &= \exp\left(\frac{1}{2}\nabla^2\delta\tau - (\hat{\mathbf{V}} - E_0)\delta\tau\right) \\ &= \exp\left(\frac{1}{2}\nabla^2\delta\tau\right) \exp(-(\hat{\mathbf{V}} - E_0)\delta\tau) \\ &\quad + \mathcal{O}(\delta\tau^2),\end{aligned}$$

which reads *diffusion* and *weighting*.

Problem: Requires a priori knowledge of the exact ground state energy E_0 .

Problem: Requires a priori knowledge of the exact ground state energy E_0 .

Solution: Introduce a *trial energy* $E_T(\tau)$ instead of E_0 in the Green's function.

Problem: The Green's function has singular points in the Coulomb interaction.

Problem: The Green's function has singular points in the Coulomb interaction.

Solution: By evolving $f(\mathbf{r}, \tau) = \Phi(\mathbf{r}, \tau)\Psi_T(\mathbf{r})$ instead of $\Phi(\mathbf{r}, \tau)$ alone, the singularities are *implicitly* taken care of.

Originally $\Phi(\mathbf{r}, \tau) = \langle \mathbf{r} | \hat{\mathbf{P}}(\tau) | \Psi_T \rangle$ solves:

$$\frac{\partial \Phi(\mathbf{r}, \tau)}{\partial \tau} = \left[\frac{1}{2} \nabla^2 - (\hat{\mathbf{V}} - E_T) \right] \Phi(\mathbf{r}, \tau).$$

Originally $\Phi(\mathbf{r}, \tau) = \langle \mathbf{r} | \hat{\mathbf{P}}(\tau) | \Psi_T \rangle$ solves:

$$\frac{\partial \Phi(\mathbf{r}, \tau)}{\partial \tau} = \left[\frac{1}{2} \nabla^2 - (\hat{\mathbf{V}} - E_T) \right] \Phi(\mathbf{r}, \tau).$$

Importance sampled:

$$\frac{\partial f(\mathbf{r}, \tau)}{\partial \tau} = \left[\frac{1}{2} \nabla \cdot (\nabla - \mathbf{F}(\mathbf{r})) - (E_L(\mathbf{r}) - E_T) \right] f(\mathbf{r}, \tau),$$

where

$$\mathbf{F}(\mathbf{r}) = 2\Psi_T(\mathbf{r})^{-1} \nabla \Psi_T(\mathbf{r})$$

is the *quantum force* and

$$E_L(\mathbf{r}) = \Psi_T(\mathbf{r})^{-1} \hat{\mathbf{H}} \Psi_T(\mathbf{r})$$

is the *local energy*.

The Green's functions have closed form solutions on the form

$$G_{\text{Diff}}(\mathbf{r}', \mathbf{r}; \delta\tau) \propto \exp\left(-|\mathbf{r} - \mathbf{r}' - D\delta\tau\mathbf{F}(\mathbf{r})|^2 / 4D\delta\tau\right),$$

$$G_W(\mathbf{r}', \mathbf{r}; \delta\tau) \propto \exp\left(-\left(\frac{1}{2} [E_L(\mathbf{r}) + E_L(\mathbf{r}')] - E_T\right)\delta\tau\right),$$

where W denotes *weighting*.

The Green's functions have closed form solutions on the form

$$G_{\text{Diff}}(\mathbf{r}', \mathbf{r}; \delta\tau) \propto \exp\left(-|\mathbf{r} - \mathbf{r}' - D\delta\tau\mathbf{F}(\mathbf{r})|^2 / 4D\delta\tau\right),$$

$$G_W(\mathbf{r}', \mathbf{r}; \delta\tau) \propto \exp\left(-\left(\frac{1}{2} [E_L(\mathbf{r}) + E_L(\mathbf{r}')] - E_T\right)\delta\tau\right),$$

where W denotes *weighting*.

$\Psi_T(\mathbf{r})$ is tailored to cancel singularities in $E_L(\mathbf{r})$.

The Markov process

Problem: The distribution $f(\mathbf{r}, \tau) = \Phi(\mathbf{r}, \tau)\Psi_T(\mathbf{r})$ is not exclusively positive unless the nodes (zeros) of $\Psi_T(\mathbf{r})$ matches those of $\Phi(\mathbf{r}, \tau)$.

The Markov process

Problem: The distribution $f(\mathbf{r}, \tau) = \Phi(\mathbf{r}, \tau)\Psi_T(\mathbf{r})$ is not exclusively positive unless the nodes (zeros) of $\Psi_T(\mathbf{r})$ matches those of $\Phi(\mathbf{r}, \tau)$.

Solution: Fixing the nodes of $f(\mathbf{r}, \tau)$ to match those of $\Psi_T(\mathbf{r})$ (the *fixed node approximation*).

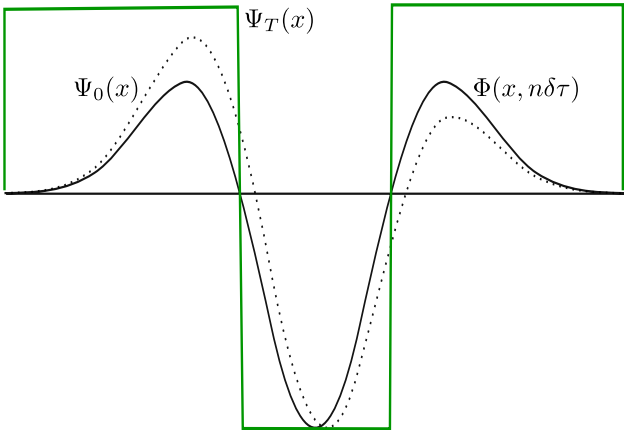


Figure: The fixed node approximation illustrated. The nodes of $\Phi(x, n\delta\tau)$ is fixed to match those of $\Psi_T(x)$.

Branching

Idea: The weights are modelled by spawning and killing walkers with a rate equal to G_W .

Branching

Idea: The weights are modelled by spawning and killing walkers with a rate equal to G_W .

Problem: G_W is not necessarily an integer.

Branching

Idea: The weights are modelled by spawning and killing walkers with a rate equal to G_W .

Problem: G_W is not necessarily an integer.

Solution: The walker branch floor(G_B) times with a chance of one additional copy.

If zero branches, the walker is removed.

Branching

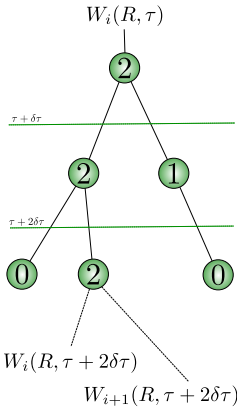


Figure: Branching illustrated. The integer values represent \bar{G}_B .

Diffusion

According to the introduced diffusion process, the new position \mathbf{r}_{i+1} is calculated from the old one, \mathbf{r}_i , as follows

$$\mathbf{r}_{i+1} = \mathbf{r}_i + D\delta\tau\mathbf{F}(\mathbf{r}_i) + \xi,$$

where ξ is a vector of normal distributed random numbers with variance $\sqrt{2D\delta\tau}$.

Diffusion

Problem: Due to a finite time step, the previous equations do not guarantee convergence.

Diffusion

Problem: Due to a finite time step, the previous equations do not guarantee convergence.

Solution: The *Metropolis algorithm* will correct this bias:

$$A(i \rightarrow j) = \min\{R_G(i \rightarrow j)R_\psi(i \rightarrow j)^2, 1\},$$

where $i \rightarrow j$ denotes a transition from state i to state j , A is the probability of accepting the transition,

$$R_G(i \rightarrow j) = G_{\text{Diff}}(\mathbf{r}_j, \mathbf{r}_i; \delta\tau) / G_{\text{Diff}}(\mathbf{r}_i, \mathbf{r}_j; \delta\tau),$$

and

$$R_\psi(i \rightarrow j) = |\Psi_T(\mathbf{r}_j)/\Psi_T(\mathbf{r}_i)|.$$

Recap

- The distribution at any stage is given as the histogram of the walkers' configurations.

Recap

- The distribution at any stage is given as the histogram of the walkers' configurations.
- The projection process involves diffusing the walkers and calculating weights.

Recap

- The distribution at any stage is given as the histogram of the walkers' configurations.
- The projection process involves diffusing the walkers and calculating weights.
- Efficient sampling by using the quantum force.

Recap

- The distribution at any stage is given as the histogram of the walkers' configurations.
- The projection process involves diffusing the walkers and calculating weights.
- Efficient sampling by using the quantum force.
- Unbiased sampling by using the Metropolis algorithm.

Recap

- The distribution at any stage is given as the histogram of the walkers' configurations.
- The projection process involves diffusing the walkers and calculating weights.
- Efficient sampling by using the quantum force.
- Unbiased sampling by using the Metropolis algorithm.
- Transition from $|\Psi_T|^2 \rightarrow f(\mathbf{r}, \tau)$ by including the weights.

Variational Monte-Carlo

Neglecting the branching results in a method known as *Variational Monte-Carlo* (VMC).

Variational Monte-Carlo

Neglecting the branching results in a method known as *Variational Monte-Carlo* (VMC).

Corresponds to calculating $\langle \Psi_T | \hat{\mathbf{H}} | \Psi_T \rangle$ using a standard Monte-Carlo approach

$$\langle \Psi_T | \hat{\mathbf{H}} | \Psi_T \rangle = \int_{\mathbf{r}} |\Psi_T(\mathbf{r})|^2 E_L(\mathbf{r}) d\mathbf{r} \simeq \frac{1}{N} \sum_{i=1}^N \frac{1}{\Psi_T(\mathbf{r}_i)} \hat{\mathbf{H}} \Psi_T(\mathbf{r}_i)$$

Variational Monte-Carlo

Variational Monte-Carlo will always result in an energy which is greater or equal to the exact ground state energy

$$\begin{aligned}\langle \Psi_T | \hat{\mathbf{H}} | \Psi_T \rangle &= \sum_{ij} C_i^* C_j \underbrace{\langle \Psi_i | \hat{\mathbf{H}} | \Psi_j \rangle}_{E_i \delta_{ij}} \\ &= \sum_i |C_i|^2 E_i \\ &= \sum_i |C_i|^2 (E_0 + \Delta E_i) \\ &= E_0 \underbrace{\sum_i |C_i|^2}_1 + \underbrace{\sum_i |C_i|^2 \Delta E_i}_{\geq 0} \\ &\geq E_0.\end{aligned}$$

Limitations: VMC

VMC is extremely robust, however, extremely dependent on a good ansatz for $\Psi_T(\mathbf{r})$.

Limitations: VMC

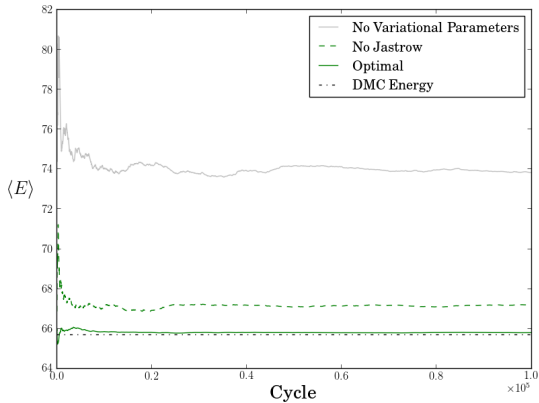


Figure: Comparison of different trial wave functions for a two-dimensional 12-particle quantum dot with unit frequency.

Diffusion Monte-Carlo

Including both diffusion and branching results in a method known as *Diffusion Monte-Carlo* (DMC).

Diffusion Monte-Carlo

Including both diffusion and branching results in a method known as *Diffusion Monte-Carlo* (DMC).

The DMC energy corresponds to the following integral

$$E_{\text{DMC}} = \frac{\int_{\mathbf{r}} f(\mathbf{r}, \tau) \frac{1}{\Psi_T(\mathbf{r})} \hat{\mathbf{H}} \Psi_T(\mathbf{r}) d\mathbf{r}}{\int_{\mathbf{r}} f(\mathbf{r}, \tau) d\mathbf{r}} = \frac{\langle \Phi(\tau) | \hat{\mathbf{H}} | \Psi_T \rangle}{\langle \Phi(\tau) | \Psi_T \rangle},$$

Diffusion Monte-Carlo

Including both diffusion and branching results in a method known as *Diffusion Monte-Carlo* (DMC).

The DMC energy corresponds to the following integral

$$E_{\text{DMC}} = \frac{\int_{\mathbf{r}} f(\mathbf{r}, \tau) \frac{1}{\Psi_T(\mathbf{r})} \hat{\mathbf{H}} \Psi_T(\mathbf{r}) d\mathbf{r}}{\int_{\mathbf{r}} f(\mathbf{r}, \tau) d\mathbf{r}} = \frac{\langle \Phi(\tau) | \hat{\mathbf{H}} | \Psi_T \rangle}{\langle \Phi(\tau) | \Psi_T \rangle},$$

which upon convergence of the projection results in
 $\hat{\mathbf{H}} |\Phi(\tau)\rangle = E_0 |\Phi(\tau)\rangle$. The energy becomes

$$E_{\text{DMC}} = \frac{\langle \Phi(\tau) | E_0 | \Psi_T \rangle}{\langle \Phi(\tau) | \Psi_T \rangle} = E_0.$$

Limitations: DMC

As discussed previously: The fixed node approximation.

Limitations: DMC

As discussed previously: The fixed node approximation.

The branching can get out of control for high *variance* systems.

Limitations: DMC

As discussed previously: The fixed node approximation.

The branching can get out of control for high *variance* systems.

Can be countered by choosing a lower time step.

$$G_W \sim \exp(\sigma(E)\delta\tau)$$

Limitations: DMC

As discussed previously: The fixed node approximation.

The branching can get out of control for high *variance* systems.

Can be countered by choosing a lower time step.

$$G_W \sim \exp(\sigma(E)\delta\tau)$$

Low $\delta\tau$ means slower convergence. Unable to span the whole space.

Limitations: DMC

Diffusion Monte-Carlo is not as dependent on the trial wave function as VMC.

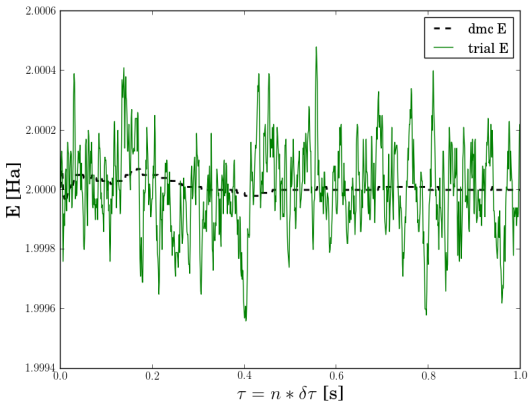


Figure: DMC calculation without the exact wave function. The exact result is $E_0 = 2$. The VMC energy is $2.0042(3)$, whereas the DMC energy is $2.00000(2)$.

The modelled systems

- Quantum dots: Confined electrons
 - Two dimensions
 - Three dimensions
 - Double wells

The modelled systems

- Quantum dots: Confined electrons
 - Two dimensions
 - Three dimensions
 - Double wells
- Atomic systems
 - Atoms
 - Homonuclear Diatomic Molecules

Quantum dots

Model the confinement using a harmonic oscillator potential

$$V_{\text{ext}}(\mathbf{r}) = \frac{1}{2}\omega^2 r^2,$$

where ω is the oscillator frequency.

Quantum dots

Model the confinement using a harmonic oscillator potential

$$V_{\text{ext}}(\mathbf{r}) = \frac{1}{2}\omega^2 r^2,$$

where ω is the oscillator frequency.

The harmonic oscillator eigenfunctions are

$$\phi_{n_x, n_y, n_z}(\mathbf{r}) = H_{n_x}(\sqrt{\omega}x)H_{n_y}(\sqrt{\omega}y)H_{n_z}(\sqrt{\omega}z)e^{-\frac{1}{2}\omega r^2},$$

which serves as the starting ground for creating an ansatz for $\Psi_T(\mathbf{r})$.

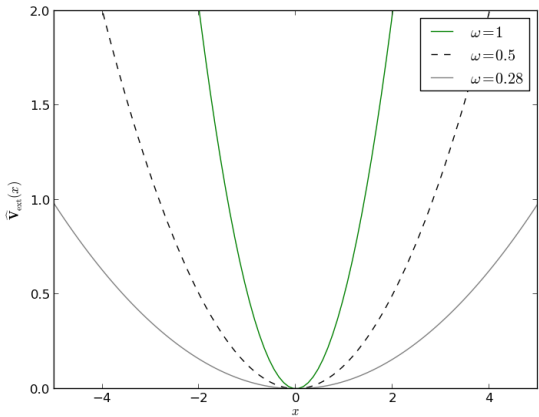


Figure: A one-dimensional version of the single-particle potential of quantum dots.

Double wells

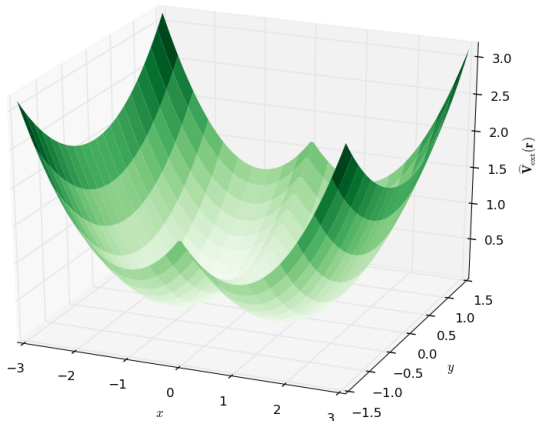


Figure: The external potential for a double-well quantum dot.

Atomic systems

Atoms are modelled with a Coulomb interaction between the electrons and the nucleus

$$V_{\text{ext}}(\mathbf{r}) = -\frac{Z}{r}. \quad (1)$$

The nucleus is fixed at the origin (the *Born-Oppenheimer Approximation*).

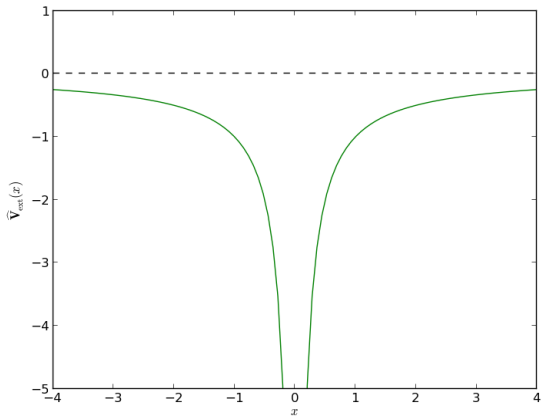


Figure: The one-dimensional version of the single-particle potential of hydrogen.

The eigenfunctions are

$$\phi_{nlm}(r, \theta, \phi; Z) \propto r^l e^{-Zr/n} \left[L_{n-l-1}^{2l+1} \left(\frac{2r}{n} Z \right) \right] Y_l^m(\theta, \phi).$$

$L_{q-p}^p(x)$: *Associated Laguerre polynomials*

$Y_l^m(\theta, \phi)$: *Spherical harmonics.*

Issue: The spherical harmonics are complex functions.

Issue: The spherical harmonics are complex functions.

Solution: Use the *solid harmonics*

$$S_l^m(r, \theta, \phi) \propto r^l [Y_l^m(\theta, \phi) + (-1)^m Y_l^{-m}(\theta, \phi)] \quad (2)$$

$$\propto r^l P_l^{|m|}(\cos \theta) \begin{cases} \cos m\phi & m \geq 0 \\ \sin |m|\phi & m < 0 \end{cases}. \quad (3)$$

The resulting eigenfunctions become

$$\phi_{nlm}(r, \theta, \phi; Z) \propto e^{-Zr/n} \left[L_{n-l-1}^{2l+1} \left(\frac{2r}{n} Z \right) \right] S_l^m(r, \theta, \phi) \equiv \phi_{nlm}^H(\mathbf{r}).$$

Molecules

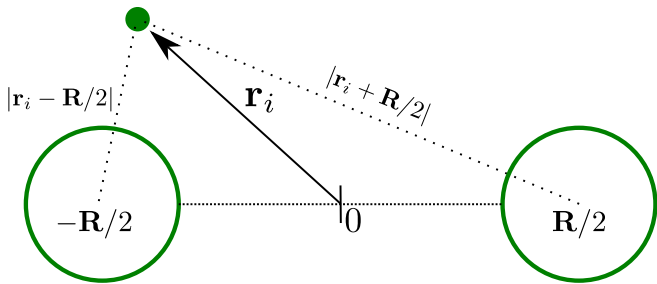


Figure: The model for the diatomic molecule.

Molecules

The Hamiltonian describing the homonuclear diatomic molecules becomes

$$\hat{\mathbf{H}}_{\text{Mol.}}(\mathbf{r}, \mathbf{R}) = \sum_{i=1}^N \left[-\frac{1}{2} \nabla_i^2 + \frac{Z}{|\mathbf{r}_i + \mathbf{R}/2|} + \frac{Z}{|\mathbf{r}_i - \mathbf{R}/2|} \right] + \frac{Z^2}{R} + \sum_{i < j} \frac{1}{r_{ij}}.$$

A transformation of the single-nucleus hydrogen eigenstates are needed:

$$\begin{aligned}\phi_{nlm}^+(\mathbf{r}_i, \mathbf{R}) &= \phi_{nlm}^H(\mathbf{r}_i + \mathbf{R}/2) + \phi_{nlm}^H(\mathbf{r}_i - \mathbf{R}/2), \\ \phi_{nlm}^-(\mathbf{r}_i, \mathbf{R}) &= \phi_{nlm}^H(\mathbf{r}_i + \mathbf{R}/2) - \phi_{nlm}^H(\mathbf{r}_i - \mathbf{R}/2).\end{aligned}$$

A transformation of the single-nucleus hydrogen eigenstates are needed:

$$\begin{aligned}\phi_{nlm}^+(\mathbf{r}_i, \mathbf{R}) &= \phi_{nlm}^H(\mathbf{r}_i + \mathbf{R}/2) + \phi_{nlm}^H(\mathbf{r}_i - \mathbf{R}/2), \\ \phi_{nlm}^-(\mathbf{r}_i, \mathbf{R}) &= \phi_{nlm}^H(\mathbf{r}_i + \mathbf{R}/2) - \phi_{nlm}^H(\mathbf{r}_i - \mathbf{R}/2).\end{aligned}$$

The same transformation is used to transform the harmonic oscillator eigenfunctions into the double well basis.

ω	E _{VMC}	E _{DMC}	E _{FCI}
0.01	0.07406(5)	0.073839(2)	0.07383505
0.1	0.44130(5)	0.44079(1)	0.44079191
0.28	1.02215(5)	1.02164(1)	1.0216441
0.5	1.66021(5)	1.65977(1)	1.6597723
1.0	3.00030(5)	3.00000(1)	3.0000001

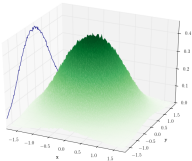
Figure: Two-particle results for two-dimensional quantum dots compared with FCI results by Veronica K.B. Olsen.

N	ω	E _{VMC}	E _{EDMC}	E _{SRG}	E _{CCSD}
42	0.1	107.881(1)	107.6389(2)	-	111.7170 {8}
	0.28	220.161(1)	219.8426(2)	219.8836 {14}	222.1401 {8}
	0.5	331.002(1)	330.6306(2)	330.6485 {14}	331.8901 {8}
	1.0	544.2(8)	542.9428(8)	542.9528 {14}	543.1155 {18}
56	0.1	176.269(2)	175.9553(7)	-	186.1034 {9}
	0.28	358.594(2)	358.145(2)	-	363.2048 {9}
	0.5	538.5(6)	537.353(2)	-	540.3430 {9}
	1	880.2(7)	879.3986(6)	-	879.6386 {17}

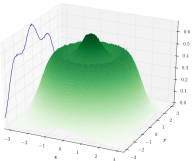
Figure: Results for two-dimensional quantum dots 42 and 56 particles compared with SRG results by Sarah Reimann and CCSD results by Christoffer Hirth.

N	ω	E _{VMC}	E _{DMC}	E ₀
2	0.01	0.07939(3)	0.079206(3)	-
	0.1	0.50024(8)	0.499997(3)	0.5
	0.28	1.20173(5)	1.201725(2)	-
	0.5	2.000005(2)	2.000000(2)	2.0
	1.0	3.73032(8)	3.730123(3)	-
8	0.1	5.7130(6)	5.7028(1)	-
	0.28	12.2040(8)	12.1927(1)	-
	0.5	18.9750(7)	18.9611(1)	-
	1.0	32.6842(8)	32.6680(1)	-
20	0.1	27.316(2)	27.2717(2)	-
	0.28	56.440(2)	56.3868(2)	-
	0.5	85.714(2)	85.6555(2)	-
	1.0	142.951(2)	142.8875(2)	-

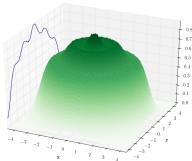
Figure: Results for three-dimensional quantum dots compared with exact solutions by M. Taut.



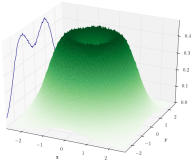
$N = 2$



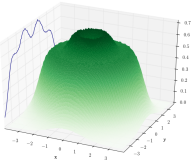
$N = 12$



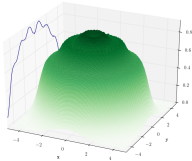
$N = 30$



$N = 6$



$N = 20$



$N = 42$

Figure: DMC one-body densities for two-dimensional quantum dots.

VMC density $|\Psi_T(\mathbf{r})|^2$

DMC density $\Phi(\mathbf{r}, \tau)\Psi_T(\mathbf{r})$

Pure density $|\Phi(\mathbf{r}, \tau)|^2$

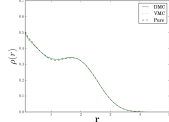
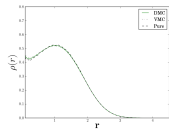
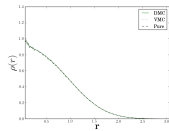
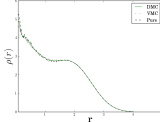
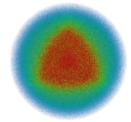
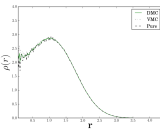
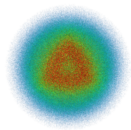
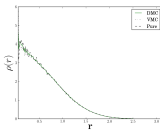
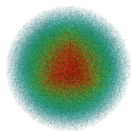


Figure: One-body densities for two- and three-dimensional quantum dots.

Lowering the frequency

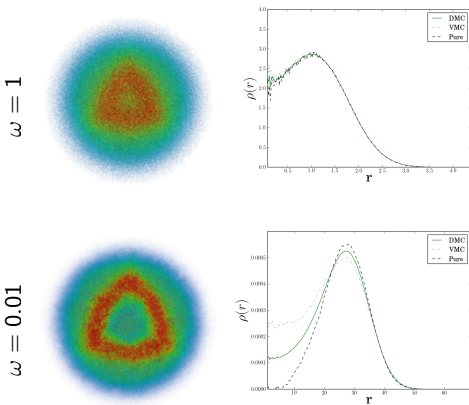
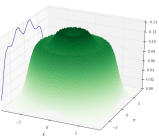
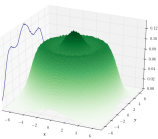
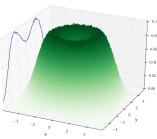
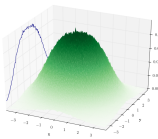
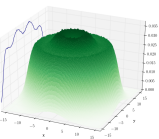
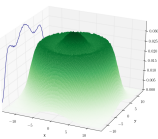
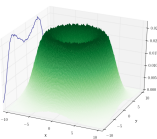
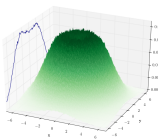


Figure: One-body densities for a 8-particle three-dimensional quantum dot for high and low frequencies.

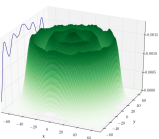
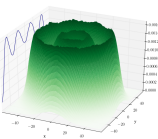
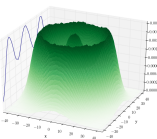
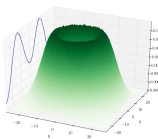
$\omega = 0.28$



$\omega = 0.1$



$\omega = 0.01$



$N = 2$

$N = 6$

$N = 12$

$N = 20$

The electrons become more *localized* and dilute.

The electrons become more *localized* and dilute.

The two- and three-dimensional densities no longer match.

The electrons become more *localized* and dilute.

The two- and three-dimensional densities no longer match.

Transition into a new region?

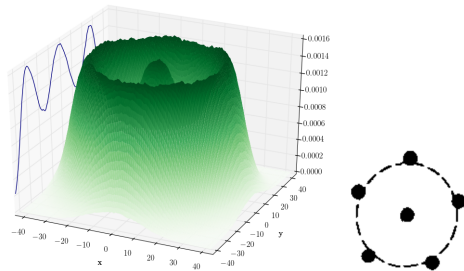


Figure: OBD for a 6-particle two-dimensional quantum dot compared to the classical theoretical configuration taken from F. Bolton, U. Rössler. *Superlattices and microstructures* **13**, 139 (1993).

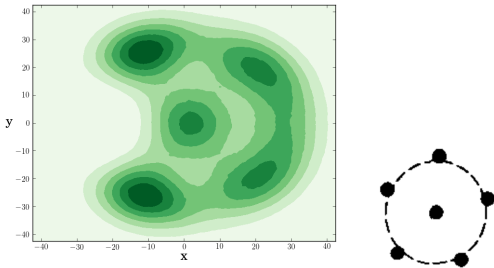


Figure: OBD for a 6-particle two-dimensional quantum dot compared to the classical theoretical configuration taken from F. Bolton, U. Rössler. *Superlattices and microstructures* **13**, 139 (1993).

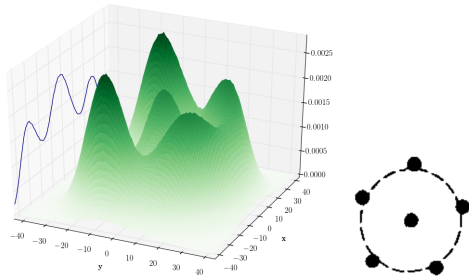


Figure: OBD for a 6-particle two-dimensional quantum dot compared to the classical theoretical configuration taken from F. Bolton, U. Rössler. *Superlattices and microstructures* **13**, 139 (1993).

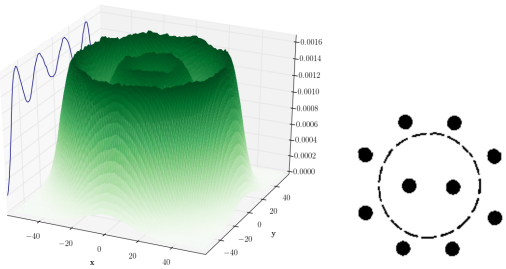


Figure: OBD for a 12-particle two-dimensional quantum dot compared to the classical theoretical configuration taken from F. Bolton, U. Rössler. *Superlattices and microstructures* **13**, 139 (1993).

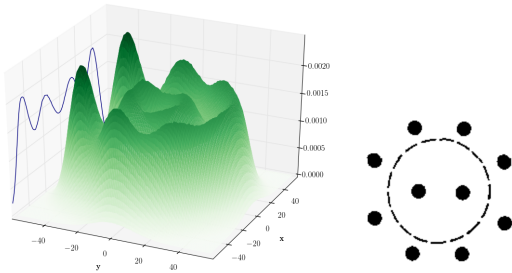


Figure: OBD for a 12-particle two-dimensional quantum dot compared to the classical theoretical configuration taken from F. Bolton, U. Rössler. *Superlattices and microstructures* **13**, 139 (1993).

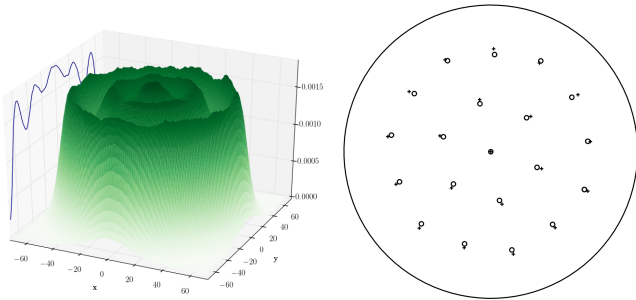


Figure: OBD for a 20-particle two-dimensional quantum dot compared to the classical theoretical configuration taken from P. Galatola et al. *Eur. Phys. J. B* **50**, 549 (2006).

This effect is called *Wigner Crystallization* and is expected for low density electron gases when the **kinetic energy on average becomes far lower than the corresponding total potential energy.**

This effect is called *Wigner Crystallization* and is expected for low density electron gases when the **kinetic energy on average becomes far lower than the corresponding total potential energy.**

The connection between potential and kinetic energy is given by the *virial theorem*

$$V(\mathbf{r}) \propto r^\gamma \quad \longrightarrow \quad \langle \hat{\mathbf{T}} \rangle = \frac{\gamma}{2} \langle \hat{\mathbf{V}} \rangle, \quad (4)$$

This effect is called *Wigner Crystallization* and is expected for low density electron gases when the **kinetic energy on average becomes far lower than the corresponding total potential energy**.

The connection between potential and kinetic energy is given by the *virial theorem*

$$V(r) \propto r^\gamma \quad \longrightarrow \quad \langle \hat{\mathbf{T}} \rangle = \frac{\gamma}{2} \langle \hat{\mathbf{V}} \rangle, \quad (4)$$

Systems with similar proportionality constant follow the same effective potential, that is, they have similar eigenstates.

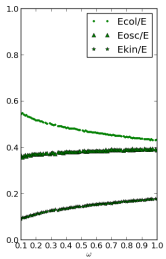
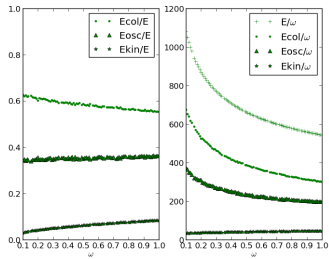
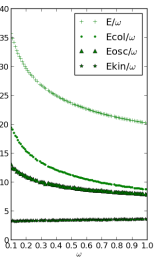
 $N = 6$  $N = 42$

Figure: The relative magnitude of the expectation value of the different energy sources as a function of the frequency ω (left) together with the magnitude of the sources' energy contributions scaled with the oscillator frequency (right).

Conclusions:

Conclusions:

The kinetic energy falls whereas the total potential energy increases.

Conclusions:

The kinetic energy falls whereas the total potential energy increases.

The kinetic energy is proportional to the frequency

$$\langle \hat{T} \rangle \propto \omega. \quad (5)$$

Transition into a Wigner crystal?

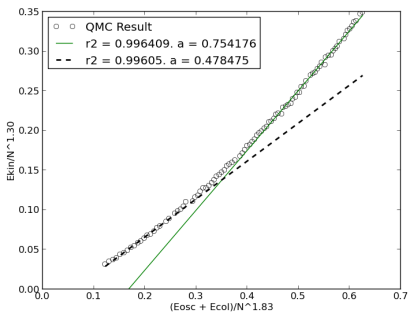
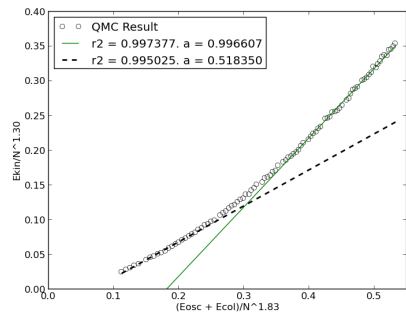
 $N = 6$  $N = 42$

Figure: The total kinetic energy vs. the total potential energy of two dimensional quantum dots. NB: Collapsed.

Preliminary double-well density

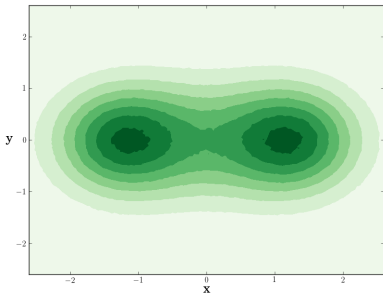


Figure: A countour plot of the trial wave function for a two-particle double-well quantum dot with the wells separated at a distance $R = 2$.

Atom	E_{VMC}	E_{DMC}	Expt.
He	-2.8903(2)	-2.9036(2)	-2.9037
Be	-14.145(2)	-14.657(2)	-14.6674
Ne	-127.853(2)	-128.765(4)	-128.9383
Mg	-197.269(3)	-199.904(8)	-200.054
Ar	-524.16(7)	-527.30(4)	-527.544
Kr	-2700(5)	-2749.9(2)	-2752.054976

Table: Ground state energies for atoms calculated using Variational - and Diffusion Monte-Carlo.

Quantum dots results for VMC and DMC were significantly more similar.

Quantum dots results for VMC and DMC were significantly more similar.

Worse for the non-noble gases and for higher number of particles.

Quantum dots results for VMC and DMC were significantly more similar.

Worse for the non-noble gases and for higher number of particles.

Easier to excite an electron into the next sub-shell (next l) than to the next n .

Quantum dots results for VMC and DMC were significantly more similar.

Worse for the non-noble gases and for higher number of particles.

Easier to excite an electron into the next sub-shell (next l) than to the next n .

The hydrogenic ansatz only accounts for *bound states*.

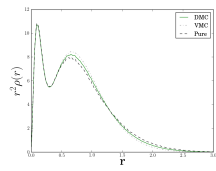
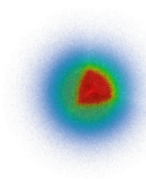
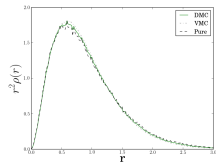
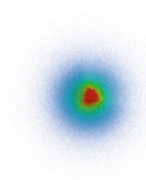


Figure: One-body densities for noble gases. Counting top to bottom:
Helium and neon.

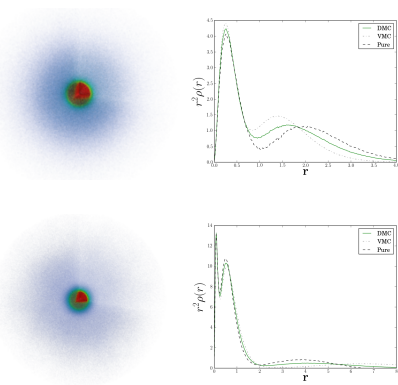


Figure: Three dimensional one-body density for alkaline earth metals;
beryllium (top) and magnesium (bottom).

Molecule	R	E_{VMC}	E_{DMC}	Expt.
H ₂	1.4	-1.1551(3)	-1.1745(3)	-1.1746
Li ₂	5.051	-14.743(3)	-14.988(2)	-14.99544
Be ₂	4.63	-28.666(5)	-29.301(5)	-29.33854(5)
B ₂	3.005	-47.746(7)	-49.155(5)	-49.4184
C ₂	2.3481	-72.590(8)	-74.95(1)	-75.923(5)
N ₂	2.068	-102.78(1)	-106.05(2)	-109.5423
O ₂	2.282	-143.97(2)	-148.53(2)	-150.3268

Table: Ground state energies for homonuclear diatomic molecules calculated using VMC and DMC.

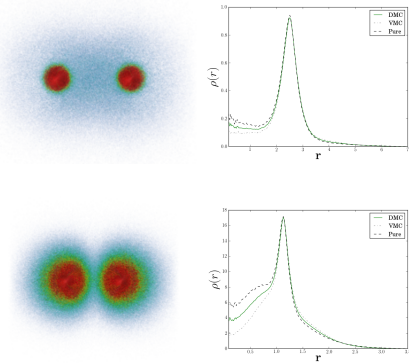


Figure: One-body densities of Li₂ (top) and O₂ (bottom).

Parameterizing Force-field Potentials

The potential energy in a molecular dynamics simulation is *any energy source which can be used to alter the kinetic energy of the atoms.*

Parameterizing Force-field Potentials

The potential energy in a molecular dynamics simulation is *any energy source which can be used to alter the kinetic energy of the atoms.*

The electrons are not simulated, hence the *total energy of the quantum mechanical system correspond to the molecular potential.*

$$F_{\text{MD}}(R) = \frac{dV_{\text{MD}}}{dR} = \frac{dE}{dR}. \quad (6)$$

Parameterizing Force-field Potentials

The potential energy in a molecular dynamics simulation is *any energy source which can be used to alter the kinetic energy of the atoms.*

The electrons are not simulated, hence the *total energy of the quantum mechanical system correspond to the molecular potential.*

$$F_{\text{MD}}(R) = \frac{dV_{\text{MD}}}{dR} = \frac{dE}{dR}. \quad (6)$$

This energy vs. R relation can be parameterized using Quantum Monte-Carlo.

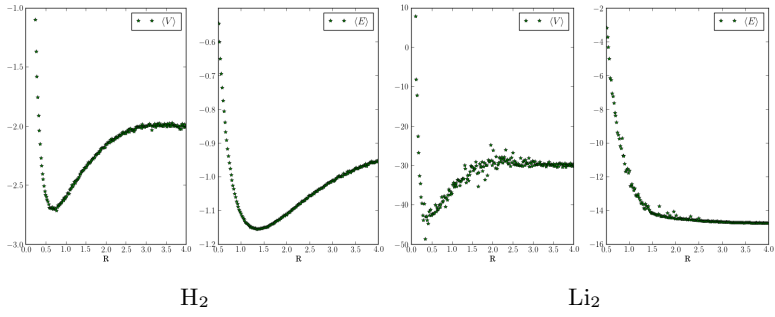


Figure: Top figures: The distance between the atoms R vs. the potential and total energy calculated using QMC.

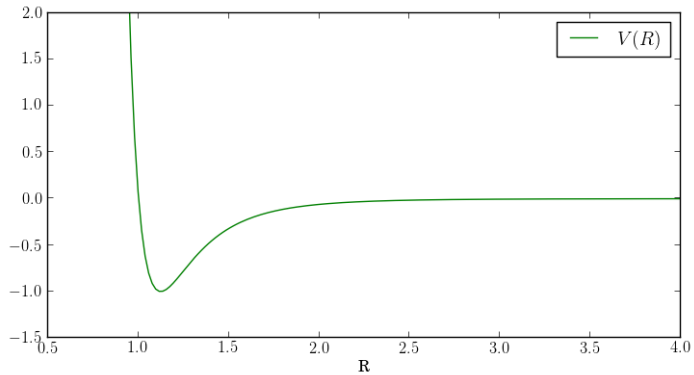


Figure: The Lennard-Jones 12-6 potential.